MICROWAVE AND HARD X-RAY DIAGNOSTICS OF NONTHERMAL ELECTRONS IN A SOLAR BURST

G. J. Hurford, D. E. Gary and J. W. Bromley
Solar Astronomy 264-33, Caltech, Pasadena, CA 91125

INTRODUCTION

In principle, the microwave brightness temperature spectrum provides a direct indication of the ambient solar magnetic field and the column density and spectral index of the nonthermal electron population accelerated in solar flares.

This paper presents the most complete application of these diagnostics to date, made possible by the simple microwave spatial structure of the flare which occurred at 1626 UT on 18 July 1988.

Microwave data were obtained at 45 frequencies between 1 and 18 GHz by the Owens Valley Solar Array, operating with three antennas. Hard X-ray spectra were obtained by the HXRBS experiment on SMM.

OBSERVATIONS

Figure 1 shows the light curve in hard X-rays with 1-second time resolution, and at 5 GHz with 10 seconds time resolution.

The analysis presented here will concentrate on the spectra at the peak of the flare.

Figure 2 shows the time evolution of the hard X-ray photon spectrum. Note that the photon spectral index was 4, implying a thick target electron spectral index of 5.

Figure 3 shows the microwave amplitude spectra as seen by projected baselines of length 244, 459 and 670 meters, respectively. Note the simple spectral shape and the reduction in amplitude at longer baselines. Closure phases indicated a simple spatial profile, dominated by a single source.

The source size is determined by noting the amplitude variation as a function of baseline. This is illustrated for a typical frequency in Figure 4, where the straight lines correspond to Gaussian source models of various FWHM diameters. It shows that the diameter can be determined to about 10%.

Having determined the diameter at each frequency, we can plot the size spectrum as shown in Figure 5a. Assuming the source is circularly symmetric, we can then determine the brightness temperature spectrum (Figure 5b). Note that the source size decreases steadily as frequency increases up to about 8 GHz. At higher frequencies, the source size may be independent of frequency. The brightness temperature spectrum (which corresponds to the center of the source) should be compared to expectations for various emission mechanisms as shown in Figure 6. Clearly the emission mechanism in this case is nonthermal gyrosynchrotron.

The nonthermal gyrosynchrotron mechanism with an electron spectral index of 5 (given by HXRBS) fully determines the *shape* of the microwave brightness temperature spectrum. The only degrees of freedom are the peak temperature and peak frequency. The resulting fit to the brightness temperature spectrum is shown in Figure 7. Discrepancies are seen at the 30% level and may be due in part to the assumption that the sources were circularly symmetric.

The parameters of the brightness temperature spectrum fit indicate an ambient magnetic field of 50 gauss and a column density of 9×10^{37} electrons cm^{-2} above 10 keV.

Using the measured source diameter of 6 arcseconds, this implies a total electron content above 25 keV at the peak of the flare of 2×10^{36} electrons.

This is consistent with the thick target electron count above 25 keV as obtained from HXRBS, which is 3×10^{35} electrons s^{-1} at the peak for a flare total of $\sim 10^{37}$ electrons.

SOURCE SIZE VARIATION WITH FREQUENCY

The variation in source diameter with frequency shown in Figure 5a clearly implies a spatial variation in source parameters. Two possibilities are a spatial gradient in magnetic field strength and/or in energetic electron density. In the case of the former, it can be shown that a bifurcated source structure would result. Since this was not observed, we postulate that the source size variation is due to spatial variation of the column density, NL, of the energetic electrons.

In Figure 8, we show the predicted brightness temperature at various frequencies as a function of position, scanning across the source. It is assumed that the magnetic field is 50 gauss, and that NL has an exponential profile indicated in the top panel with 6 arcsec FWHM.

Note that at high frequecies, the microwave source size accurately reflects the energetic electron distribution. At low frequencies, however, the microwave source size can greatly exceed the size scale of the electron distribution. This is because the edge of the microwave source occurs at the point at which the source becomes optically thin. Therefore the low frequency source size can give a very misleading indication of the size scale of the energetic electron distribution.

Assuming only an exponential or gaussian NL distribution of 6 arcsec FWHM (the size indicated by the highest OVRO frequencies), and the deduced magnetic field and central value of NL, we can then predict the microwave source size as a function of frequency. This prediction is shown in Figure 9, where it is seen to reproduce the qualitative features of the observed size spectrum.

CONCLUSIONS

For an impulsive flare with a simple microwave source structure, the microwave brightness temperature spectrum matches theoretical expectations with a magnetic field strength of 50 gauss. There is quantitative consistency between the microwaves and thick target hard X-rays as to the number of energetic electrons.

The microwave source size decreased with frequency until the microwaves became optially thin. The data suggest that the nonthermal electrons were distributed over a region 6 arcseconds in diameter.

The source size variations were consistent with a model in which the column density of the energetic electrons varies with position.

This analysis suggests how spatially-resolved microwave spectroscopy can distinguish thermal from nonthermal electon distributions, can determine magnetic field and electron parameters at the center of the source, and can provide insights into the spatial gradients in these parameters.

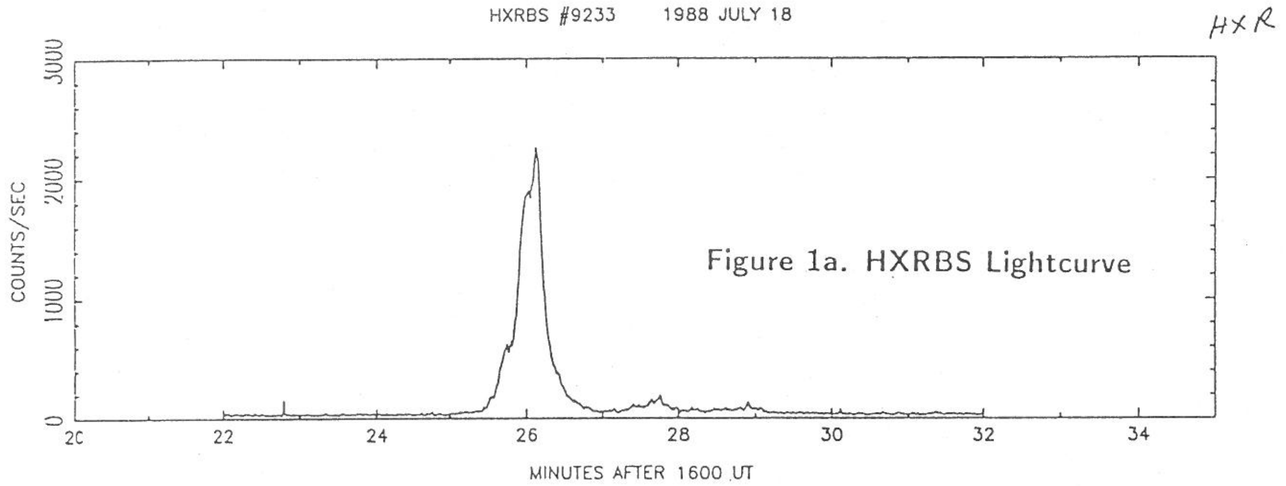

Figure 1a. HXRBS Lightcurve

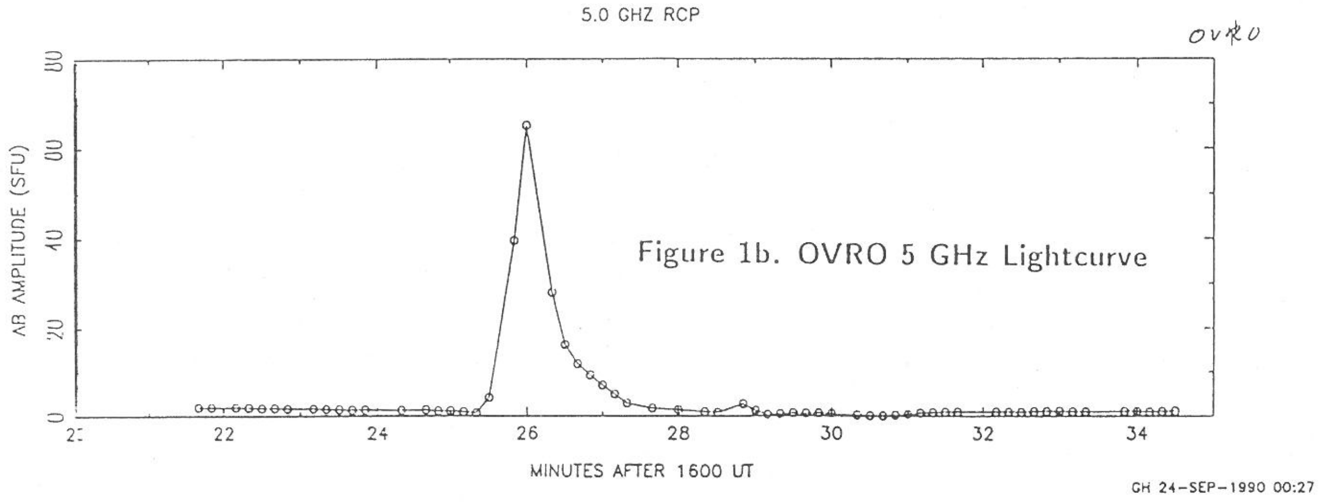

Figure 1b. OVRO 5 GHz Lightcurve

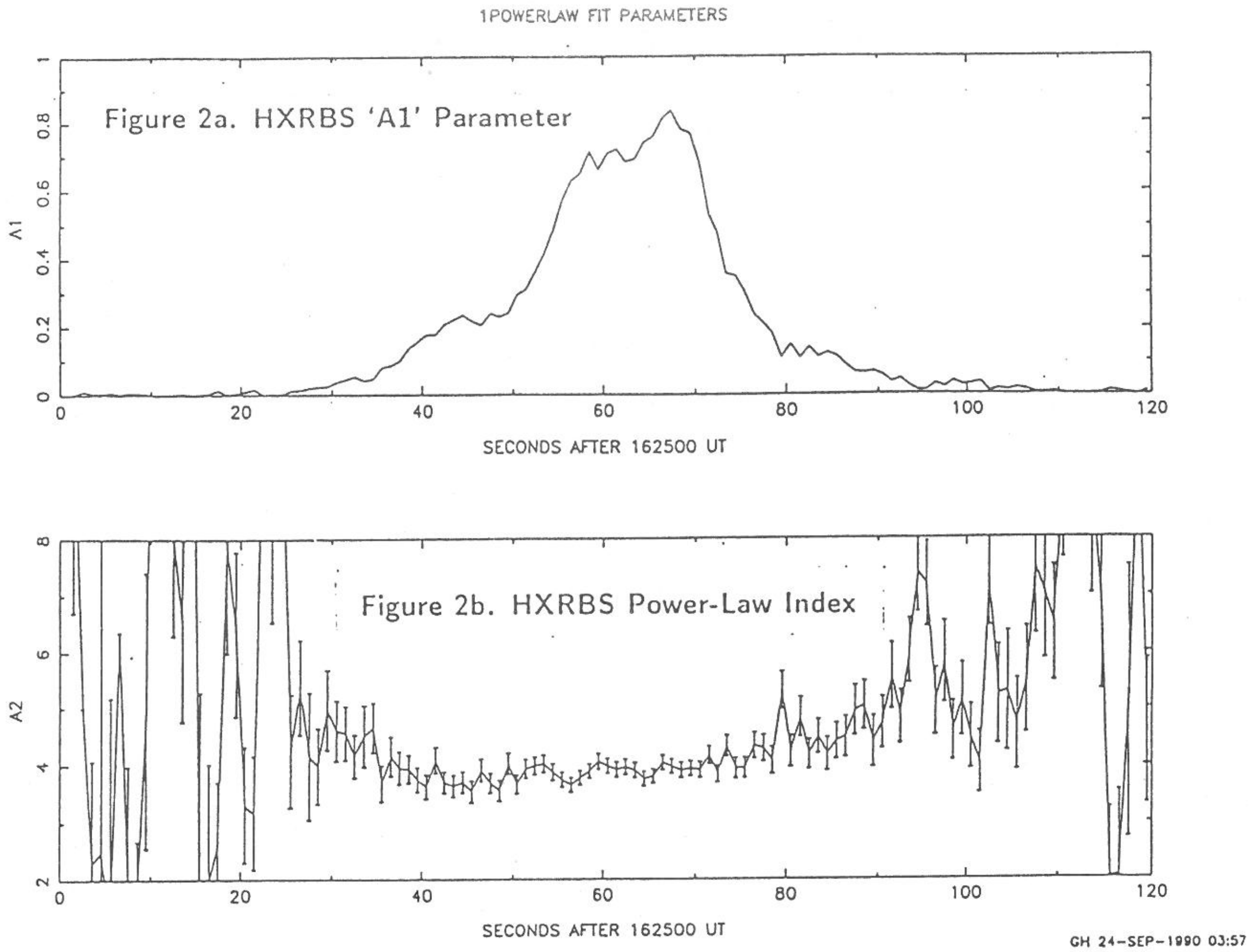

Figure 2a. HXRBS 'A1' Parameter

Figure 2b. HXRBS Power-Law Index

Figure 3. OVRO Flux Spectra

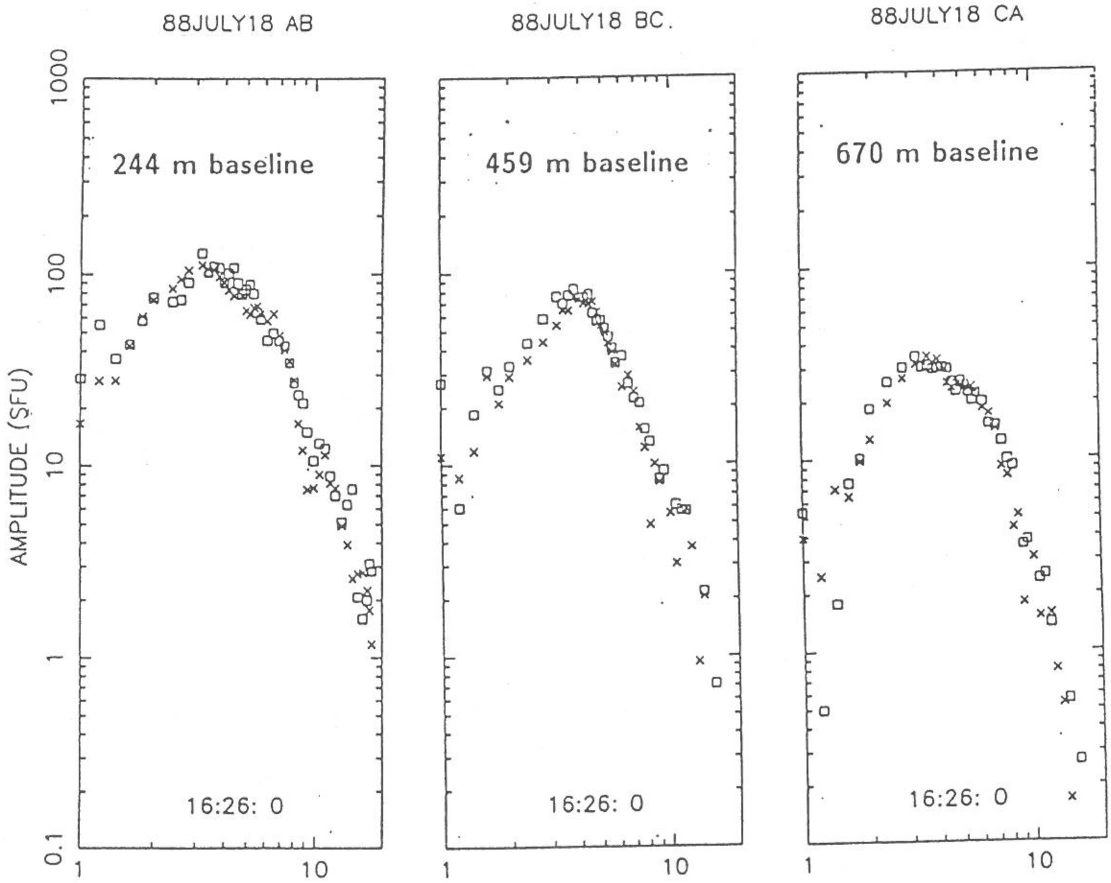

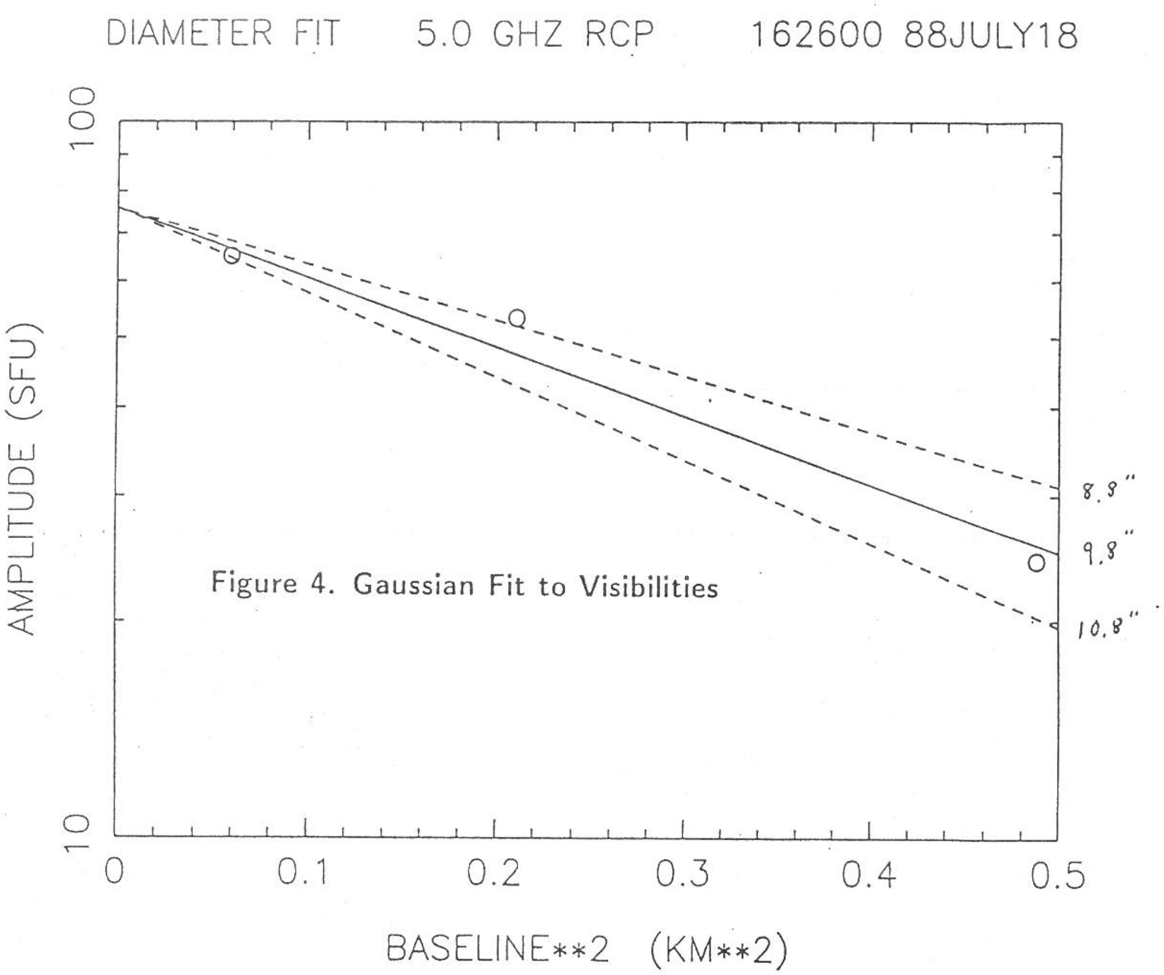

Figure 4. Gaussian Fit to Visibilities

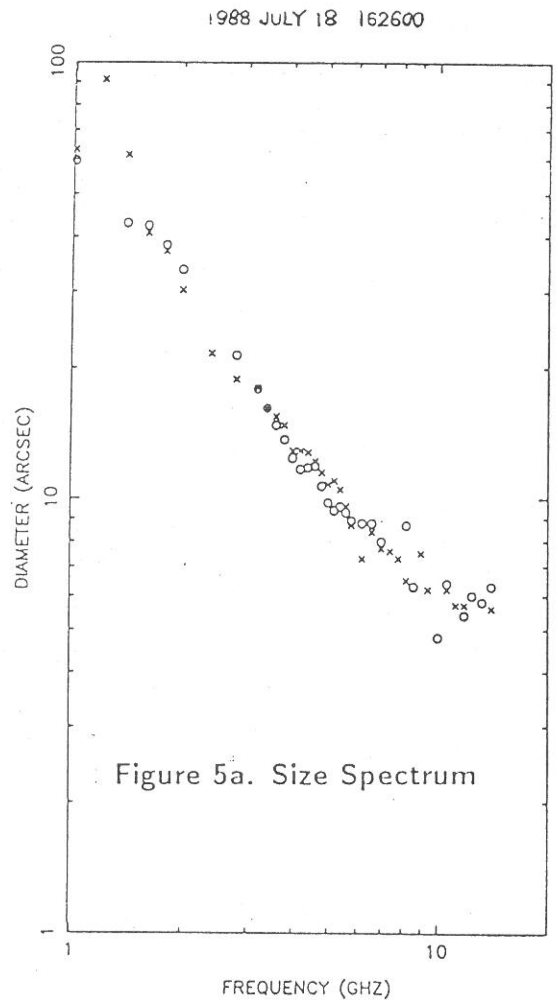

Figure 5a. Size Spectrum

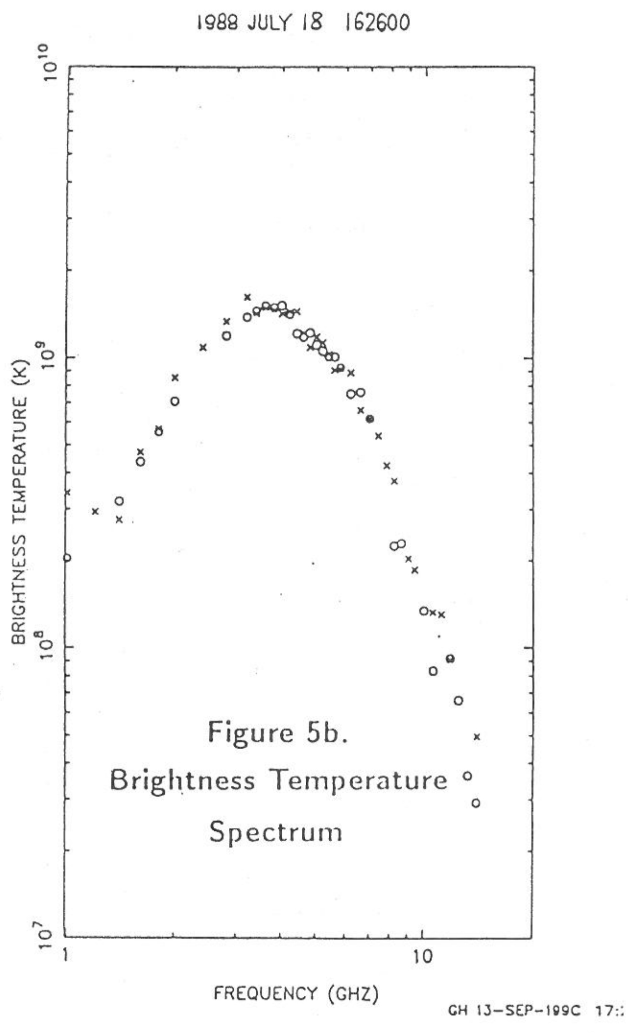

Figure 5b. Brightness Temperature Spectrum

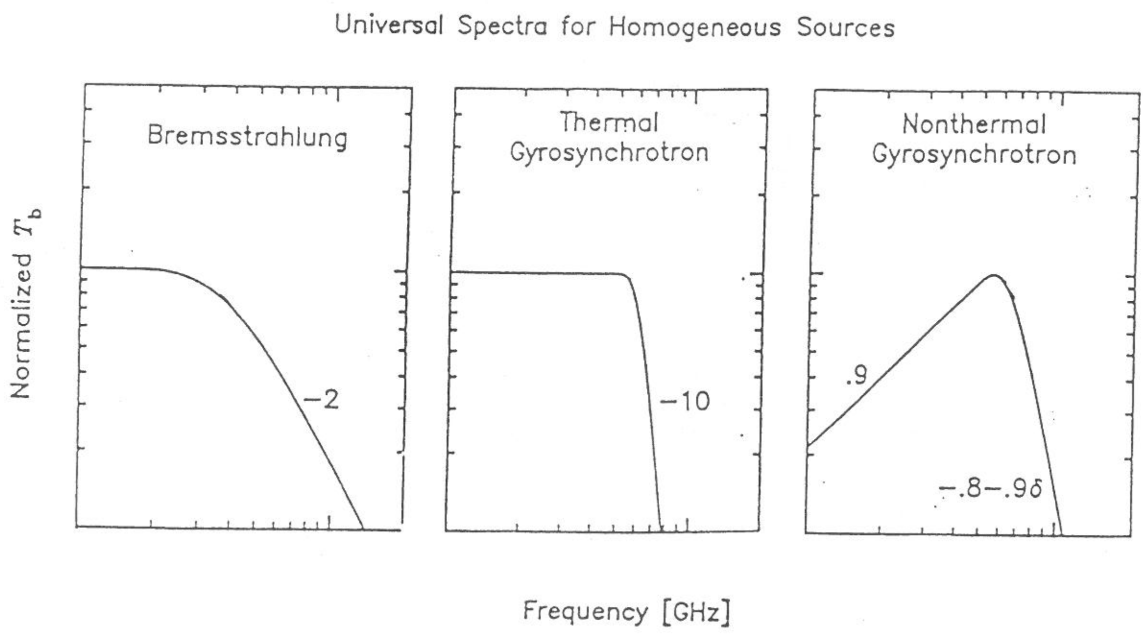

Figure 6. Spectral Shapes For Various Emission Mechanisms

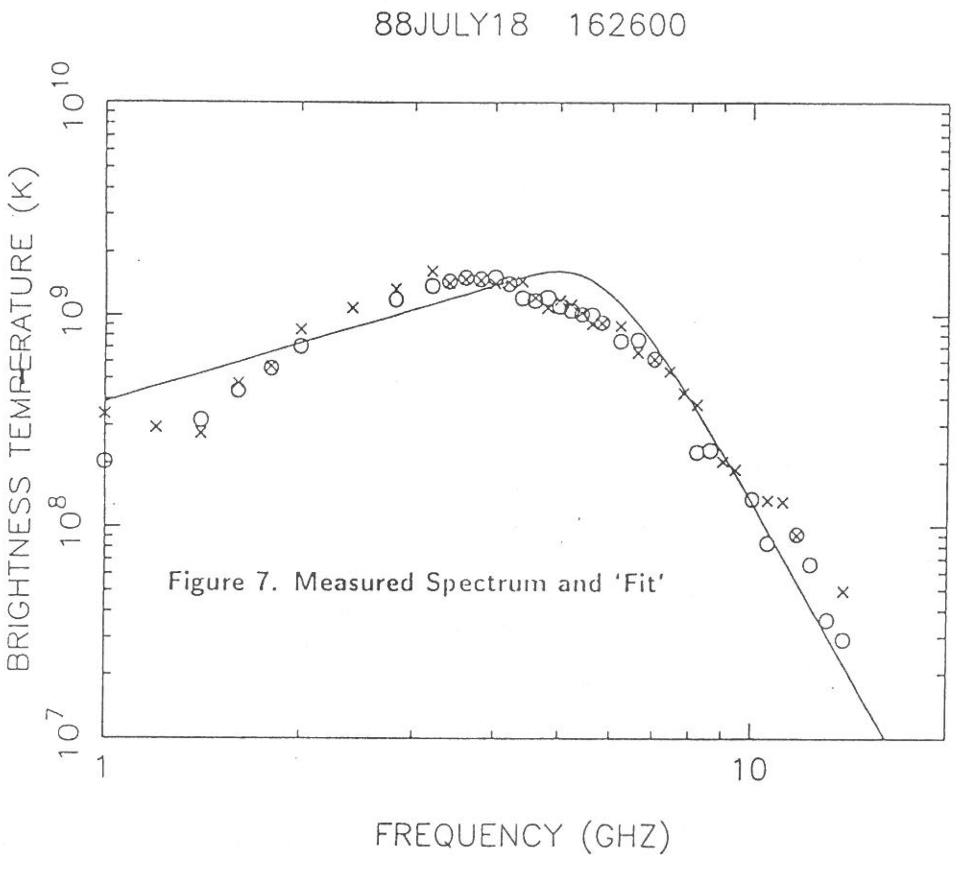

Figure 7. Measured Spectrum and 'Fit'

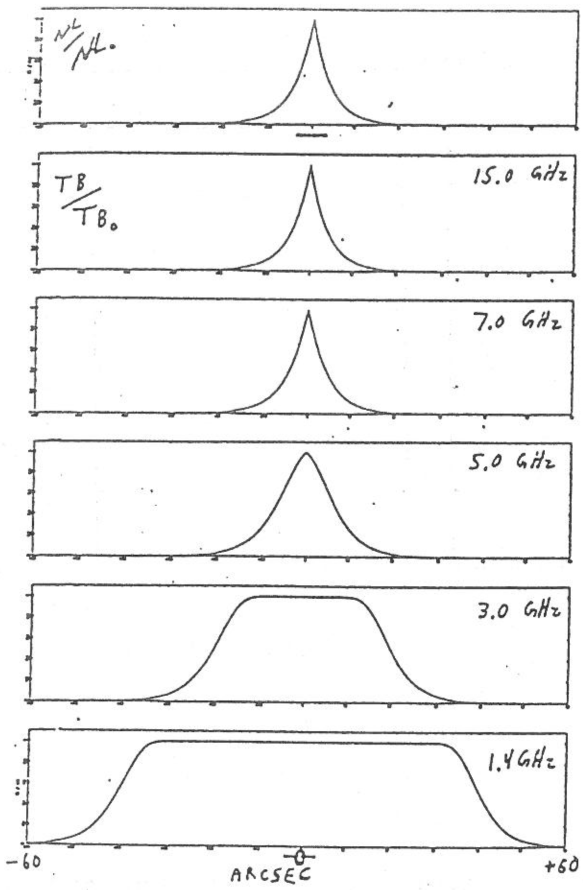

Figure 8. Spatial Variation of Brightness Temperature

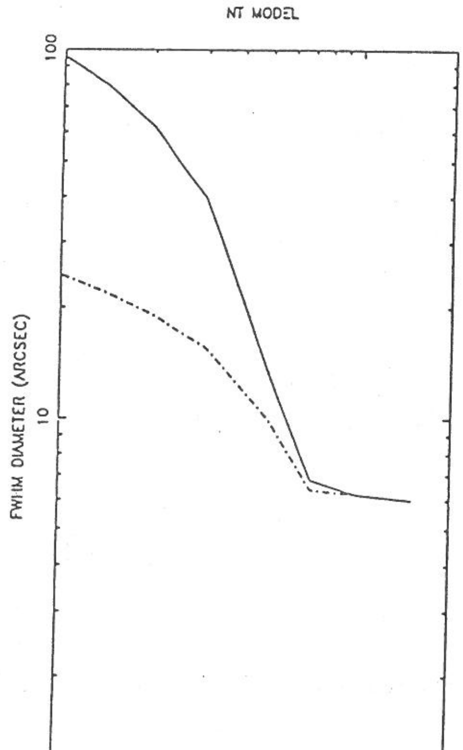

Figure 9. Predicted Size Spectrum for Two Models of Density